Comparison Of ^{82}Rb Pet Myocardial Blood Flow Computations

Andrew Van Tosh, MD;[a] Jonathan Scheiner, BA; [a] Austin Lester, LNMT; [a] Christopher J. Palestro, MD;[b] Kenneth J. Nichols, PhD[b]

St. Francis Hospital, Roslyn, NY;[a] Donald & Barbara Zucker School of Medicine at Hofstra/Northwell, Hempstead, NY[b]

BACKGROUND: There are now multiple different ^{82}Rb dynamic PET/CT algorithms available for the computation of absolute myocardial blood flow (MBF) and myocardial flow reserve (MFR = stress MBF/rest MBF). We wished to compare MBF & MFR measurements of a curve-based model to those of a retention model.

METHODS: We retrospectively analyzed ^{82}Rb PET/CT rest and regadenoson-stress data for 123 pts evaluated for known or suspected CAD. A curve-based model ("Method1," Emory University; J Nucl Cardiol 2017, doi 10.1007/s12350-017-1049-y) employed a 1-tissue compartment, 1-rate constant (microsphere analog) model with spillover effects that modelled tracer uptake in myocardial tissue to compute rest & stress MBF. A retention model ("Method2;" University of Michigan; J Nucl Cardiol 2007;14:455-65) that uses integrated images and relies less on dynamic curve shapes was applied to the same data. All computations were performed without refence one another, and blinded to other clinical information. The t-test, Mann-Whitney or Wilcoxon test were applied to assess difference among mean results, depending on whether continuous variables were normally distributed. Linear regression and Bland-Altman analyses compared MBF and MFR values between the Methods. Method1 included automated quality assurance algorithms to identify potential technically compromised time-activity curves (e.g., detector saturation, patient movement, curve width, etc.). Cases were excluded for comparison if technical problems were encountered, and if any clearly unphysiologic results were obtained.

RESULTS: Excluding data of 9 pts flagged by the QA algorithms as likely technical problems, and 4 additional cases of unphysiologic MFR values (2 cases for Method1 and 2 cases for Method2), there were 110 pts with no data quality issues. Rest & stress MBF values & MFR values were not normally distributed (Kolmogorov-Smirnov $p < 0.0001$). Rest MBF was lower for Method1 than Method2 (0.75±0.16 versus 0.84±0.24 ml/g/min, $p < 0.0001$), as was stress MBF (1.48±0.49 versus 1.66±0.67 ml/g/min, $p < 0.0001$), but MFR values were similar for the two methods (2.00±0.58 versus 2.01±0.69, $p = 0.82$). Method1 MFR correlated significantly with Method2 MFR ($r = 0.79$, $p < 0.0001$), with Bland-Altman mean difference of -0.01, ±1.96 SD limits of agreement of +0.82 to -0.85, intercept of 0.33±0.14 ($p = 0.02$) & slope of -0.17±0.07 ($p = 0.01$).

CONCLUSIONS: While rest & stress absolute myocardial blood flow values were lower for the curve-based method than for the retention-based method, the myocardial flow reserve values were essentially the same for the two techniques.

COVID-19 Immunization-Related Lymphadenopathy on FDG-PET/CT: A Single Institution Cohort Study with Proposed Recommendations

So Yeon Kim MD[1], Edgar Zamora MD2*[2], Kith Pradhan Ph.D.[1],*
Rasim Gucalp MD[1], Amit Verma MBBS[1], Kwang Chun MD[2], & Balazs Halmos MD[1]
*Co-first authors

Correspondence: Edgar Zamora, MD
Department of Oncology[1], Department of Nuclear Medicine[2]
Montefiore Medical Center
Albert Einstein College of Medicine
Bronx, NY 10461, USA
Telephone: 718-904-8505
Fax: 718-904-8501
ezamora@montefiore.org

Short title: COVID-19 Immunization Lymphadenopathy FDG-PET

Keywords:

COVID-19 vaccine, FDG-PET, lymphadenopathy, malignancy

Abstract

Background: Hypermetabolic lymphadenopathy associated with COVID-19 immunization has been observed in FDG-PET/CT. We sought to determine the incidence and imaging characteristics of vaccine-associated lymphadenopathy following COVID-19 immunization and propose guidelines for appropriate timing and interpretation of vaccination-associated FDG-avid lymphadenopathy.

Methods: We conducted a retrospective study in patients who received COVID-19 vaccines prior to FDG-PET/CT scanning from February 1st, 2021, to April 9th, 2021. We collected baseline demographics, primary indication for FDG-PET/CT, date of vaccination, and type and dose of vaccine received. We documented the incidence of FDG-avid axillary lymphadenopathy

and imaging characteristics. A 5-point scoring system was utilized to grade and normalize uptake intensity of each lymph node.

Results: Of 423 patients who underwent FDG-PET/CT, 54 had received the COVID-19 vaccine. Of the 54 patients, 35 (65%) had grade ≥ 2 axillary lymphadenopathy, of which 32 (91%) were interpreted as vaccine-associated lymphadenopathy. Patients undergoing work-up or history of lymphoid malignancies were observed to have lower incidence ($p = 0.0101$), grade ($p = 0.00817$) and number ($p = 0.0421$) of FDG-avid axillary lymphadenopathy. Younger patients were observed to have a trend towards higher grade of lymphadenopathy. The median number of post-vaccination days in patients with grade ≥ 2 lymphadenopathy was 16 (range 1-27 days) from first vaccination and 14.5 (range 5 to 66 days) from second vaccination.

Conclusions: A significant proportion of patients who underwent FDG-PET/CT following COVID-19 immunization were found to have locoregional lymphadenopathy. Proposed guidelines are presented to review current data and offer recommendations in management of vaccine-associated adenopathy.

Title

Progressive Cranial Osteolysis Associated with Gorham-Stout Syndrome: A Multi-Modality Nuclear Medicine Assessment

Chanseo Lee[1], Daniel B. Chonde[2], Simran Grewal[3], Althea D. Tapales[4], Yingbing Wang[5], Santoshi Indrakanti[5], Thomas S.C. Ng[2]

[1]Massachusetts Institute of Technology
[2]Department of Imaging, Massachusetts General Hospital, Harvard Medical School
[3]Department of Medicine, Massachusetts General Hospital, Harvard Medical School
[4]University of Vermont
[5]Department of Radiology, Massachusetts General Hospital

Background: Gorham-Stout (GS) syndrome, commonly known as the vanishing bone disease, has fewer than 300 known cases worldwide. Its cause is poorly understood. Clinical and biochemical studies have been limited to just a few cases given the rarity of this condition. Although the exact causes of the GS are unknown and less than 300 known cases exist worldwide, several case reports have described its pathological findings. The disintegrating osseous matrix is replaced by an invasive, expanding vascular tissue,[1,2,3] as well as increased lymphatic structures [4]. Areas undergoing massive osteolysis have been associated with increased osteoclastic activity and interleukin-6 concentration.[3] The primary cause of the osteolysis is thought to be abnormal lymphangiogenesis.[5] This process can be associated with pain, swelling, and even impairment of the affected area.[1] Treatment of GS can take many forms, including surgery, radiation, and pharmaceuticals.[6] In particular, medications that have been used to treat this process include rapamycin (an immunosuppresant) [7,] denosumab (an inhibitor of a tumor necrosis factor) [9] , as well as biphosphonate (which stabilizes bone resorption) .[4,6,10]. Future pharmaceutical approaches to treatment will depend on a better understanding of GS-associated lymphangiogenesis and its biochemistry.[11]

Methods: The patient is a 58-year-old female who presented initially for wrist radiographs in the setting of trauma. A lucent lesion was noted in the wrist, raising concerns for a neoplastic process. This prompted further imaging workup with bone scintigraphy. Subsequent whole body and SPECT/CT bone scans were obtained. MRI and CT scans tracked the osteolysis over the next 6 months, and F-18 FDG-PET/CT was used to monitor metabolically active processes immediately adjacent to the skull lesion and in distant locations.

Results: Whole body scans and SPECT/CT bone scans revealed a large photopenic area in the right frontal bone with increased peripheral uptake. This corresponded to an area where the patient reported a sensation of “fullness”. Image guided biopsy at that location further revealed fibrous dysplasia suggestive of weakening bone. The patient’s MRI scans depict the disappearance of the patient’s frontal bone. Otherwise, F-18 FDG PET images show no detrimental effects on brain activity nor abnormal uptake elsewhere. Transverse and sagittal CT scans over a 6-month period show minimal progression, although focal areas showed some increased tapering of the bone lesion characteristic of this disease.[1] The current patient remains on rapamycin without significant symptoms. Continued follow clinical and imaging follow up is being pursued.

Conclusions: Various scintigraphy methods can be used to monitor the osteolytic development of Gorham-Stout disease. Despite what little is known about this disease’s origins and treatment, this case report demonstrates that these methods are important for both diagnosis and development of image-guided treatment plans for patients.

References

1. Nikolaou VS. Vanishing bone disease (Gorham-Stout Syndrome): A review of a rare entity. World Journal of Orthopedics. 2014;5:694.
2. Dickson GR, Hamilton A, Hayes D, et al. An investigation of vanishing bone disease. Bone. 1990;11:205–210.
3. Devlin RD, Bone HG, Roodman GD. Interleukin-6: A potential mediator of the massive osteolysis in patients with Gorham-Stout Disease. The Journal of Clinical Endocrinology & Metabolism. 1996;81:1893–1897.
4. Hammer F, Kenn W, Wesselmann U, et al. Gorham-Stout Disease-Stabilization During Bisphosphonate Treatment. Journal of Bone and Mineral Research. 2004;20:350–353.
5. Foult H, Goupille P, Aesch B, et al. Massive osteolysis of the cervical spine. Spine. 1995;20:1636–1639.
6. Hu P, Yuan X-gui, Hu X-yang, et al. Gorham-Stout syndrome in mainland CHINA: A case series of 67 patients and review of the literature. Journal of Zhejiang University Science B. 2013;14:729–735.
7. Liang Y, Tian R, Wang J, et al. Gorham-Stout disease successfully treated with sirolimus (rapamycin): A case report and review of the literature. BMC Musculoskeletal Disorders. 2020;21.
8. Wu Q, Zhou X, Huang D, et al. IL-6 enhances osteocyte-mediated osteoclastogenesis by Promoting JAK2 And RANKL activity in vitro. Cellular Physiology and Biochemistry. 2017;41:1360–1369.
9. Liu M, Liu W, Qiao C, et al. Mandibular Gorham–Stout disease. Medicine. 2017;96.
10. Lehmann G, Pfeil A, Böttcher J, et al. Benefit of a 17-year Long-term bisphosphonate therapy in a patient WITH Gorham–stout syndrome. Archives of Orthopaedic and Trauma Surgery. 2008;129:967–972.
11. Hardegger F, Simpson LA, Segmueller G. The syndrome of idiopathic osteolysis. classification, review, and case report. The Journal of Bone and Joint Surgery British volume. 1985;67-B:88–93.

Post-treatment Exposure Rates for Y-90 Microsphere Patients

Steven Blum[1], Eugenio Silvestrini[2 3].

Hofstra University, Hempstead, NY, USA
1 Department of Radiology, Radiation Safety, Northwell Health, Manhasset, NY, USA
3 Department of Physics and Astronomy, Hofstra University, Hempstead, NY, USA

Background:

Over the last 30 years, the use of Yttrium-90 (Y-90) in the treatment of liver tumors has seen a dramatic increase. This is especially true after the FDA approval for clinical use of Y-90 glass microspheres (TheraSpheres). Our healthcare system contains several major hospitals, and the Y-90 microsphere therapy program at our institution began in 2019. FDA approved microspheres from two companies (SiRTeX and Boston Scientific's TheraSphere) are used for these procedures; more recently, TheraSphere has been the predominant product. Our institution utilizes the exposure rate at 1 meter to determine if a patient can be released without radiation hygienic precautions; below 2 mR/hr at that distance patients can be released without ins truction. Above this threshold, patients must receive written instructions for radiation precaution.

Methods:

60 patients who received Y-90 microsphere therapy since our program began in September 2019 had their post-treatment exposure rates recorded. Before treatment began, the surface exposure rates for the liver, lungs, stomach, as well as the exposure rate at 1 m from the torso were recorded using a survey meter, and following treatment, the exposure rates at the same locations were recorded using the same survey meter.

Results:

All of the patients in this study exhibited pre-treatment exposure rates at 1 m from the torso that were indistinguishable from background. Following treatment, the maximum exposure rate and the average exposure rate at 1 m as well as the surface readings for the liver, lungs, and stomach for all 60 patients are recorded in Table 1.

Conclusions:

Of the 60 patients in this study, none showed a post-treatment exposure rate at I m from the torso larger than the 2 mR/hr release criteria. Although we are not technically required to give instructions to the patient at these levels we recorded, we do provide written hygienic precautions to the patients to help minimize exposure rates to contacts in order to comply with ALARA principles.

Key Words: Yttrium-90, Y-90, Therasphere

Table I. Exposure rates for regions of interest post-treatment for 60 patients.

Site (for organs, surface readings were recorded)	Average Reading (mR/hr)	Maximum Reading (mR/hr)
Liver	1.96	28.50
Lungs	0.68	1.77
Stomach	0.53	2.90
1 meter from torso	0.08	0.50

CASE REPORT: DELAYED IMAGING TIME TO IMPROVE QUALITY OF ^{18}F-FDG PET STUDIES FOR CARDIAC SARCOIDOSIS

Andrew Van Tosh, MD;[a] Jonathan Scheiner, BA; [a] Jaison Mathew, LNMT; [a] Christopher J. Palestro, MD;[b] Kenneth J. Nichols, PhD[b]

St. Francis Hospital, Roslyn, NY;[a] Donald & Barbara Zucker School of Medicine at Hofstra/Northwell, Hempstead, NY[b]

BACKROUND: Cardiac involvement in systemic sarcoidosis is often difficult to detect clinically but may be present in up to 40% of patients, causing arrhythmias, heart failure and death. Diagnosis using ^{18}F-FDG PET allows early institution of appropriate treatment and improves mortality. Standard PET FDG protocols for oncologic and cardiac viability studies suggest imaging 60-90 minutes after isotope injection. We present a patient case to illustrate the challenges of ^{18}F-FDG imaging of cardiac sarcoidosis.

METHODS: A 57-year old male patient developed systemic and pulmonary sarcoidosis, presumed secondary to toxic exposure as a 9/11/2001 first responder. Ventricular arrhythmias were noted, and he was referred for diagnostic imaging to evaluate possible cardiac sarcoidosis. The patient underwent a 48-hour low carbohydrate, high fat/protein diet and a 16-hour fast. All imaging was performed on a GE Discovery-710 PET/CT camera with 64 slice CT. At rest, 1.11 Gbq (30 mCi) ^{82}Rb was injected IV. First pass and list mode acquisition was begun at 90 seconds and continued for 7 minutes, immediately following which 492 Gbq (13.3) mCi ^{18}F-FDG was injected. The patient remained at rest in a quiet room. PET imaging was performed at 90 minutes post ^{18}F-FDG injection and was repeated at 150 minutes post ^{18}F-FDG injection. CT imaging was performed for attenuation correction and anatomic image correlation.

RESULTS: The ^{82}Rb images displayed an overall uniform perfusion appearance. The 90-minute ^{18}F-FDG images had considerable blood pool activity which interfered with the visualization of myocardial tracer uptake. Repeat ^{18}F-FDG imaging at 150 minutes showed clearing of blood pool activity, and an unambiguous focus of ^{18}F-FDG uptake in the basal-mid septal and lateral walls, indicating active inflammation, and consistent with a diagnosis of sarcoidosis.

CONCLUSIONS: In patients imaged for cardiac sarcoidosis at standard imaging intervals, retained blood pool activity may obscure ^{18}F-FDG tracer uptake within cardiac structures. Delaying imaging by 2.5-3 hours may allow for further blood pool clearance and increased tissue uptake, thereby improving detection of inflammation.

Incorporation of High-Risk Features Seen on PET MPI to Expedite Revascularization

Authors: *Simran Grewal DO[1], Antonio Lopez MSII[2], Azar Radfar MD PhD[3], Kenechukwu Mezue MD MSc[1], Ahmed Tawakol MD[1], Michael T. Osborne MD[1], Thomas S.C. Ng MD PhD[4]*

Affiliations: Massachusetts General Hospital, Department of Medicine, Division of Cardiology and Cardiovascular Imaging Research Center,[1] Drexel University College of Medicine,[2] University of Miami, Miller School of Medicine, Division of Cardiology,[3] Massachusetts General Hospital, Department of Imaging, Division of Nuclear Medicine and Molecular Imaging[4]

Learning Objectives:

1) In addition to perfusion data, myocardial perfusion imaging using positron emission tomography (PET-MPI) provides additional information which may elucidate the severity of coronary artery disease and the need for urgent intervention

Case: A 55-year-old man with a history of coronary artery disease (CAD) status post percutaneous coronary intervention (PCI) to the right coronary artery (RCA) and left circumflex artery (LCx) with drug-eluting stents (DES) underwent positron emission tomography myocardial perfusion imaging (PET MPI) to evaluate anginal symptoms. Pharmacological stress was induced with 400mcg of Regadenoson; imaging was performed with ^{13}N-ammonia (18.41 mCi at rest, 19.8 mCi at stress) as part of a standard clinical protocol. Summed static images revealed mild basal to mid anterior, moderate to severe anterolateral, moderate inferolateral, and moderate to severe inferior ischemia without evidence of infarction (Figure 1). The left ventricular ejection fraction (LVEF) dropped from 66% without wall motion abnormalities at rest to 51% with lateral hypokinesis and inferior hypokinesis at stress. There was transient ischemic dilation (TID) with a ratio of 1.5. Aside from the septum, peak stress myocardial blood flow (MBF) ranged from 0.7 – 0.8 ml/min/g and the myocardial flow reserve (MFR) ranged from 1.3 – 1.7 in all three coronary vascular territories (Figure 1). Subsequent invasive coronary angiography (ICA) was performed and demonstrated an 80% stenosis of the left main (LM) artery, severe ostial and 50% mid left anterior descending (LAD) stenoses, a diffusely diseased second diagonal artery (D2), 50% mid-LCx and 99% obtuse marginal (OM) 2 stenoses, and a total occlusion of the proximal RCA (Figure 2). The patient was referred for five-vessel coronary artery bypass graft (CABG) surgery with left internal mammary artery to LAD, saphenous vein graft (SVG) to D2, SVG sequentially to OM1 and OM3, and SVG to posterior descending artery.

Impact/Discussion: PET MPI clearly depicted significant ischemia involving the aforementioned territories, suggesting multivessel CAD as the etiology of the findings. Other key findings provided further support for this conclusion. For example, the decline in LVEF during stress raises the concern for severe obstructive CAD and is often indicative of post-ischemic stunning. In addition, TID is hypothesized to occur due to global myocardial ischemia and a value greater than 1.13 is considered a high-risk feature[1]. Finally, stress MBF below 1.8 ml/min/g and MFR below 2.0 throughout most of the myocardium provided further support for multi-territory ischemia and greater cardiovascular risk. Our patient demonstrated these high-risk features, and this data led to expedited ICA that corroborated PET MPI findings and subsequent revascularization via CABG.

Conclusion: PET MPI not only provides high quality imaging data but also provides additional information that provides improved risk stratification and diagnostic performance in severe multi-vessel disease.

References:

1) Dorbala S, Di Carli MF. Cardiac PET perfusion: prognosis, risk stratification, and clinical management. *Semin Nucl Med*. 2014;44(5):344-357. doi:10.1053/j.semnuclmed.2014.05.003

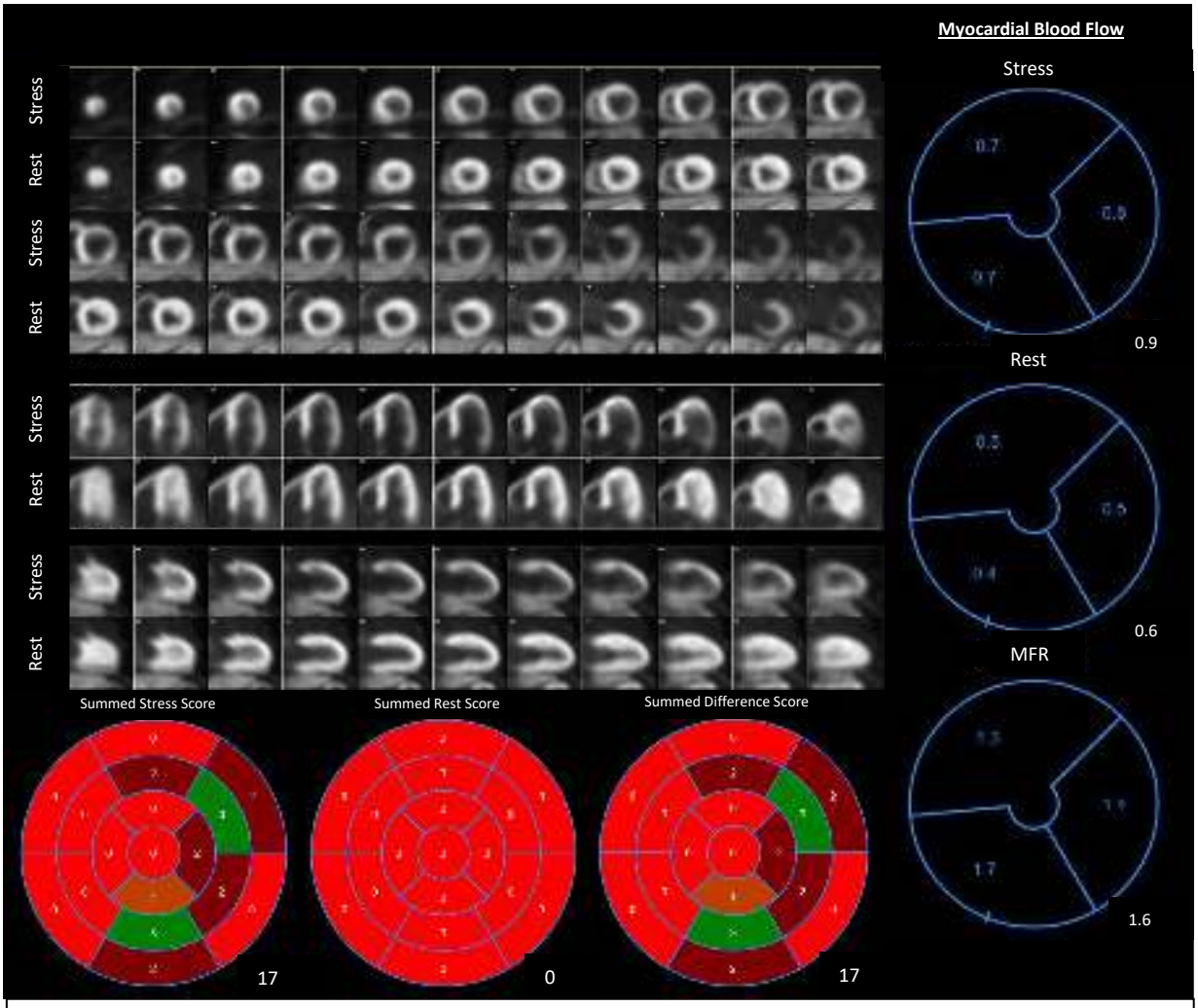

Figure 1: Black and white summed perfusion images along with polar maps showing extensive territories of ischemia (left) and myocardial blood flow quantification at rest and stress (top and middle in units of ml/min/g) and myocardial flow reserve (bottom) showing diffusely decreased peak stress myocardial blood flow and myocardial flow reserve.

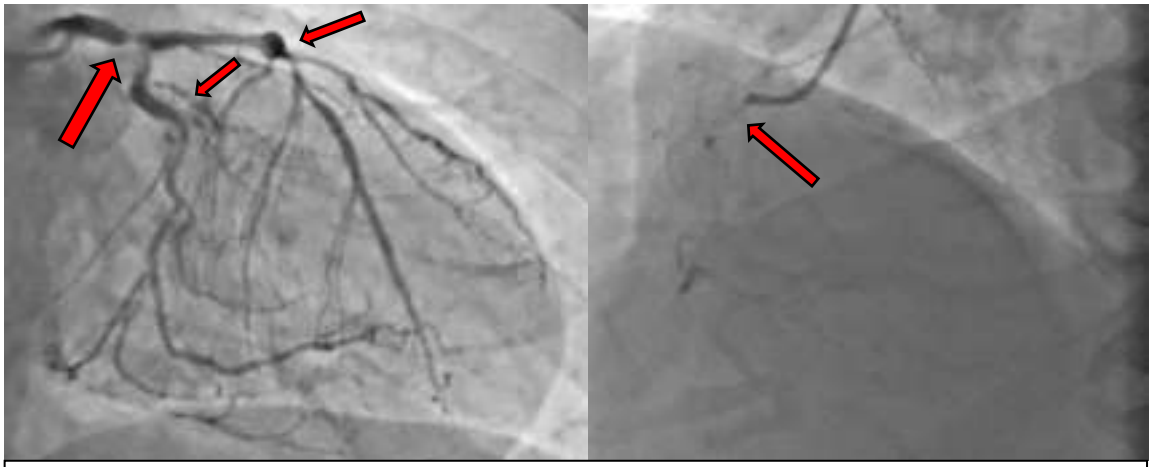

Figure 2: Invasive coronary angiography showing the diffusely diseased left coronary system (left with arrows from the left depicting left main, obtuse marginal, and left anterior descending artery stenoses) and occluded proximal right coronary artery (right, indicated by arrow).

ATA GUIDELINES: THYROID CANCER RISK ASSESSMENT AND ROLE OF I-131 ABLATION

Faisal Jamal, MD[1,2], and Rachel Powsner, MD, MPH[1,3,4]

Joint Program of Nuclear Medicine, Harvard Medical School[1], Brigham & Women's Hospital Department of Radiology[2], Boston VA Healthcare System[3], Boston University School of Medicine Department of Radiology[4]

Objective:

Summarize and review the important highlights of 2015 American Thyroid Association Management Guidelines for Adult Patients with Thyroid Nodules and Differentiated Thyroid Cancer. We discuss the pre- and post-operative risk assessment and stratification of well-differentiated thyroid cancers based on fine needle aspirate pathology, surgical findings, and post-surgical staging. The recommendations for post-operative radioiodine ablation are included as well.

Background:

Thyroid cancer incidence is increasing; it nearly tripled from ~ 5 to 14 cases per year per 100,000 between 1975-2009. This increase is partially due to increased incidental discovery of thyroid nodules on imaging such as sonography. However, only 7-15% of thyroid nodules are positive for cancer on biopsy. The diagnostic approach to the thyroid nodule including identification of the high-risk characteristics suspicious for thyroid cancers has become increasingly important to avoid unnecessary exams and treatment in benign and low risk nodules. Furthermore, risk stratification after total thyroidectomy based on TNM staging is useful to help determine the need for subsequent radioiodine ablative therapy.

Case Report:

A patient with a 4.3 cm papillary thyroid cancer and incidental finding of microscopic disease in a central neck lymph node is used to illustrate the application of the ATA guidelines including the surgical approach, post-operative radio-ablation, and likelihood of future cancer recurrence. In this case the large primary tumor size was an indication for complete thyroidectomy. The postoperative TNM staging was T3 N1a (Stage III for his age group). His ATA risk stratification was low to intermediate risk given a positive lymph node. For this risk classification post-operative radiation ablation was recommended for consideration and was generally favored. His post ablation scan combined with a normal serum thyroglobulin level placed him in an excellent response category with very low risk of recurrence.

Conclusion:

The ATA guidelines may be useful for endocrinologists, surgeons, and nuclear medicine physicians to help them determine appropriate treatment for well-differentiated thyroid cancer, both in terms of surgical approach and decision making about utility of post-operative radioiodine ablation. In addition, it provides an estimate of the risk of disease recurrence following treatment.

Lymphoma Response criteria on imaging: Important Highlights

Faisal Jamal, MD[1,2]; Muhammad Aamir Latif, MD[1,2]; Lokeshwar Reddy Chinthakunta[1,2], Hina Shah, MD[1,2]

Joint Program of Nuclear Medicine, Harvard Medical School[1],
Brigham & Women's Hospital Department of Radiology[2]
75 Francis Street, Boston, MA 02115

Corresponding author
Faisal Jamal, MD
75 Francis Street, Department of Radiology
Division of Nuclear medicine
Boston, MA 02115
Email: fjamal1@bwh.harvard.edu

Objective:

To briefly review the history of lymphoma treatment response criteria based on anatomical and functional imaging studies with particular attention to the most recent PET parameters used for this assessment. Illustrative images of lymphoma cases using Deauville scoring for response assessment in lymphoma are shown.

Background:

Lymphoma are heterogeneous lymphoproliferative malignancies with variable clinical presentation and response profiles. These are broadly categorized as Hodgkin lymphoma (HL) or non-Hodgkin lymphoma (NHL), with the latter group constituting of the majority of the cases. Response assessment, which includes cross sectional and functional imaging (PET), allows early treatment modifications during a course of chemotherapy as well as during follow-up and periods of active surveillance. The use of size criteria alone to differentiate benign from malignant lymph nodes was found to be only partially reliable, therefore functional imaging parameters, in particular 18F-FDG PET, were added to improve response assessment.

Before 1999, the use of many response criteria applied to many different imaging modalities led to inconsistent and unreliable methods of assessing treatment response to different therapies. In 1999, the National Cancer Institute created the International Working Group (IWG), which used CT based changes in the size of enlarged lymph nodes and other tumor sites as a means of assessing disease regression or progression. However, a shortcoming of CT based morphological criteria was felt to be a lack of functional/molecular imaging information. Therefore, in 2007, the International Harmonization Project (IHP) provided new recommendations which incorporated PET/CT into tumor response assessment criteria.

The Deauville Scoring System in 2009 became a standard-bearer for interim tumor response assessment, helping in predicting prognosis and allowing for early treatment modifications. This system uses qualitative grading in the form of a 5-point scale that compares relative activity in sites of tumors to the reference activity in the mediastinal blood pool and liver . Recently, the Lugano classification was introduced, which, in addition to the Deauville scoring system, applies CT sizing criteria which is particularly useful for lymphomas with low or variable FDG uptake,

Methods and Results:

We show illustrative examples of the application of Deauville scoring of lymphoma cases before and after (?mid-treatment) treatment.

Conclusion:

There has been, and continues to be, improvement in imaging criteria, both anatomical and functional, for assessment of lymphoma response to treatment. Most recently the Deauville and Lugano scoring systems are being used.

Clinical Significance of Hot Rim Sign in Hepatobiliary Scintigraphy Studies. An Educational Abstract.

Muhammad A. Latif, MD; Faisal Jamal, MD; Scott Britz-Cunningham, MD

Brigham and Women's Hospital | Harvard Medical School
Department of Radiology, Division of Nuclear Medicine
75 Francis Street, Boston, MA 02115

Corresponding Author
Muhammad A Latif, MD
75 Francis Street, Nuclear medicine Division
Boston, MA 02115
Email: mlatif@bwh.harvard.edu

Objective:

This educational abstract describes the pathophysiology, clinical significance and prognosis associated with hot rim sign seen on hepatobiliary scintigraphy.

Background:

The 'hot rim' sign has been a recognized imaging marker in hepatobiliary imaging since it was first reported in 1984. Although a secondary diagnostic feature, it can be a useful marker of disease severity, as it is associated with more severe forms of cholecystitis, such as perforated and gangrenous cholecystitis.

Pathophysiology:

On a HIDA scan, acute cholecystitis typically presents as non-visualization of the gallbladder, despite uptake elsewhere within the biliary tree or in the small bowel. The 'hot rim sign', which may at times be seen concomitant with this, depends upon an inflammatory reaction of the hepatic parenchyma adjacent to the gallbladder fossa and the subsequently resulting hyperemia. Normally, bile is produced by hepatocytes and transported through small, compressible bile canaliculi surrounding each hepatocyte. In acute cholecystitis, hepatocytes usually remain metabolically competent, and will take up radiotracer, conjugate it, and excrete it into their canaliculi. However, gallbladder distension and inflammatory edema in acute cholecystitis can compress the canaliculi nearest to the gallbladder fossa, which impedes transport of bile, and results in localized retention of tracer activity while the more distant parts of the liver wash out. The scintigraphic appearance is that of a rim of persistent activity outlining the gallbladder fossa, which increases in relative

prominence over time. When associated with nonvisualization of the gallbladder at one hour, the positive predictive value of ‘hot rim sign’ for acute cholecystitis approaches 94%. More particularly, this sign (RMS) is associated with gangrenous cholecystitis and requires urgent surgical evaluation.

Conclusions:

Nuclear medicine physicians and radiologists should be able to recognize and understand the basis for the imaging feature of the ‘hot rim sign’. When present, it can be clinically ominous, because, as an indicator of inflammatory edema, it can be associated with a higher risk of perforated or gangrenous cholecystitis, requiring urgent surgical evaluation.

Reference:

1. Biliary scintigraphy. The "hot rim" sign” M A Cawthon, D M Brown, M F Hartshorne, R D Karl Jr, J M Bauman, W H Howard 3rd, S R Bunker PMID: 6542471
2. Swayne LC, “Filippone Gallbladder perforation: correlation of cholescintigraphic and sonographic findings with the Niemeier classification. J
3. The rim sign: association with acute cholecystitis, D L Bushnell, S B Perlman, M A Wilson, R E Polcyn; PMID: 3712052

Title

Hyperostosis Frontalis on Bone Imaging Mimicking Metastatic Disease

Robert Lawson[1], Bashar Kako[1], Kenechukwu Ndubisi Mezue[2], Simran Grewal[2], Jason Lauer[1], Saurabh Rohatgi[1], Thomas S.C. Ng[1]

[1] Department of Radiology, Massachusetts General Hospital, Harvard Medical School
[2] Department of Medicine, Division of Cardiology and Cardiovascular Imaging Research Center, Massachusetts General Hospital, Harvard Medical School

Abstract

Background: Imaging plays a vital role in the staging and prognostication of patients with breast cancer. In particular, the whole-body bone scintigraphy is an especially useful tool to assess for osseous metastases. However, the imaging physician needs to be aware of mimickers of metastatic disease that may drastically alter patient management and prognostication.

Methods/Results: A 79-year-old female with a medical history notable for rheumatic mitral stenosis status post mechanical mitral valve replacement 30 years ago was admitted with congestive heart failure and found to have a peri-valvular leak around her mechanical mitral valve. As part of her work up, she had a coronary CT scan where she was noted to have a 3 cm breast mass with 1.5 cm axillary lymph nodes (Figure 1). Her most recent mammogram was obtained 5 years prior to presentation, which was normal. Family history was notable for maternal breast cancer found in her 70s. Laboratory work up was notable for elevated CA 15-3, triggering staging imaging work up with diagnostic chest, abdomen/pelvis CT and bone scan. Whole-body nuclear bone scan utilizing Technetium-99m MDP showed diffusely heterogeneous increased uptake throughout the calvarium, most prominent over the frontal bone (Figure 2) and worrisome for metastatic disease. Given the lack of any prior head imaging, head CT was subsequently performed (Figure 3). This showed diffuse thickening of the inner table, most prominent in the frontal regions, without destructive marrow replacing lesion. This finding is compatible with hyperostosis frontalis interna (HFI), and the patient was subsequently discharged for outpatient follow up with breast oncology.

Discussion: HFI is a benign thickening of the inner layer of the skull bone. It is usually asymptomatic and more commonly seen in postmenopausal women as an incidental finding [1,2]. However, in the setting of cancer, it could easily be mistaken for metastasis. The etiology of this condition is unknown but has been thought to be associated with endocrine or metabolic derangements [1,3]. A cadaveric study reported the frequency of any morphological findings of HFI at 12.5% which explains why this is often an incidental imaging finding [4]. Imaging findings on a skull radiograph include thickening and increased density of the frontal inner

table, more apparent on the lateral view [2]. CT shows bilaterally symmetric overgrowth of the inner table of the frontal and parietal bones, sparing the midline, without crossing the sagittal sinus and outer calvarial skull [5]. Nuclear medicine evaluation with bone scintigraphy is nonspecific for increased radiotracer uptake in the affected area and MRI demonstrates extra-axial lobulations that parallel fatty marrow signal on all sequences [2,5].

Although the bone scan imaging appearance of the presented patient is highly suggestive of HFI, similar appearances have represented metastatic lesions in the past [6]. Therefore, confirmatory anatomic imaging particularly by CT should be obtained if no prior correlative studies are available, as in this case. This case highlights the importance of assessing for incidental findings during imaging exams, and to broaden the differential of apparent abnormal findings in the setting of oncologic staging.

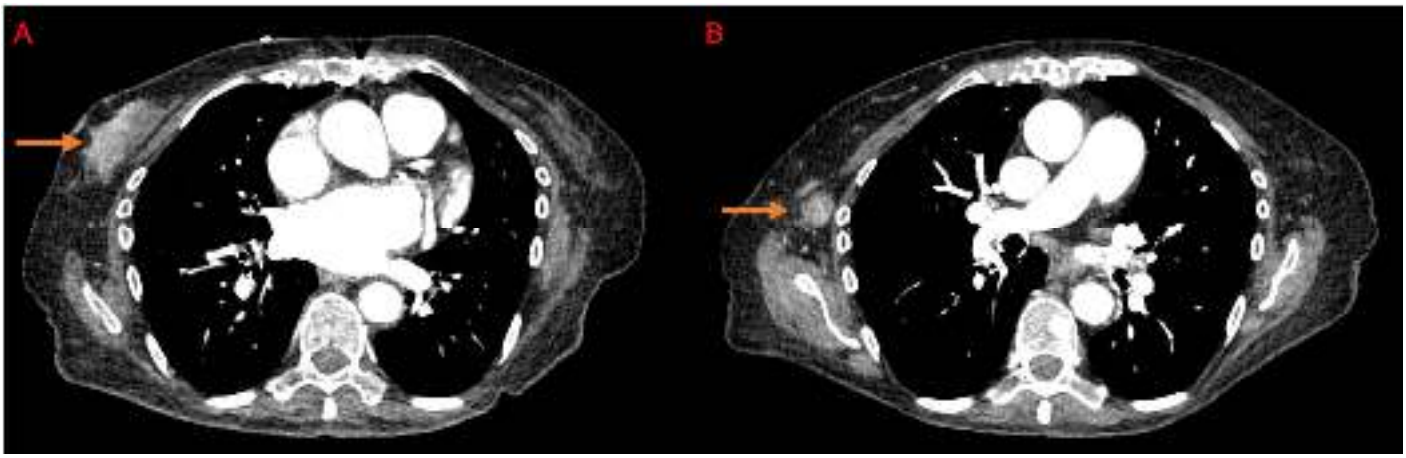

Figure 1. Coronary CT scan shows right breast mass (A) with axillary lymphadenopathy (B).

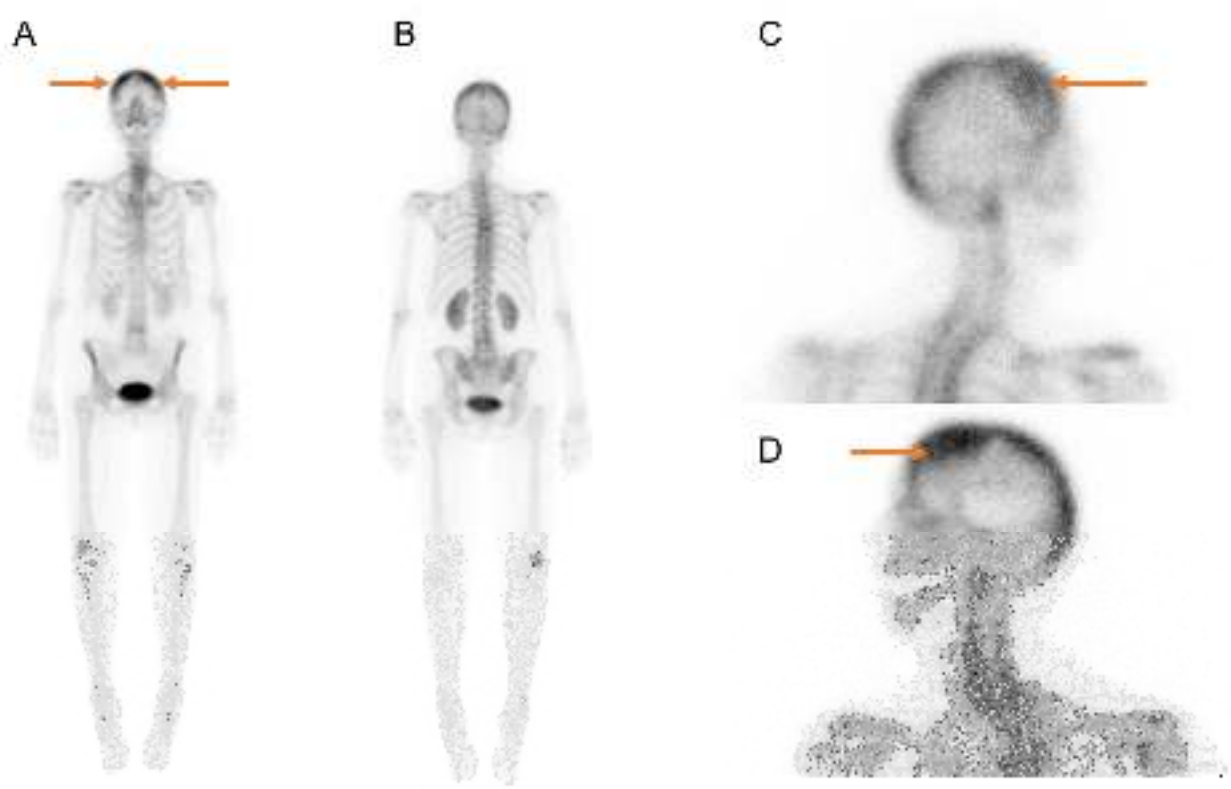

Figure 2. Whole body planar (A, B) Tc99m-MDP bone scans show degenerative changes in the right knee. Incidentally noted was diffuse increased calvarial uptake (arrows). Lateral spot views of the skull (C, D) redemonstrate this finding, with increased uptake noted especially in the frontal bone.

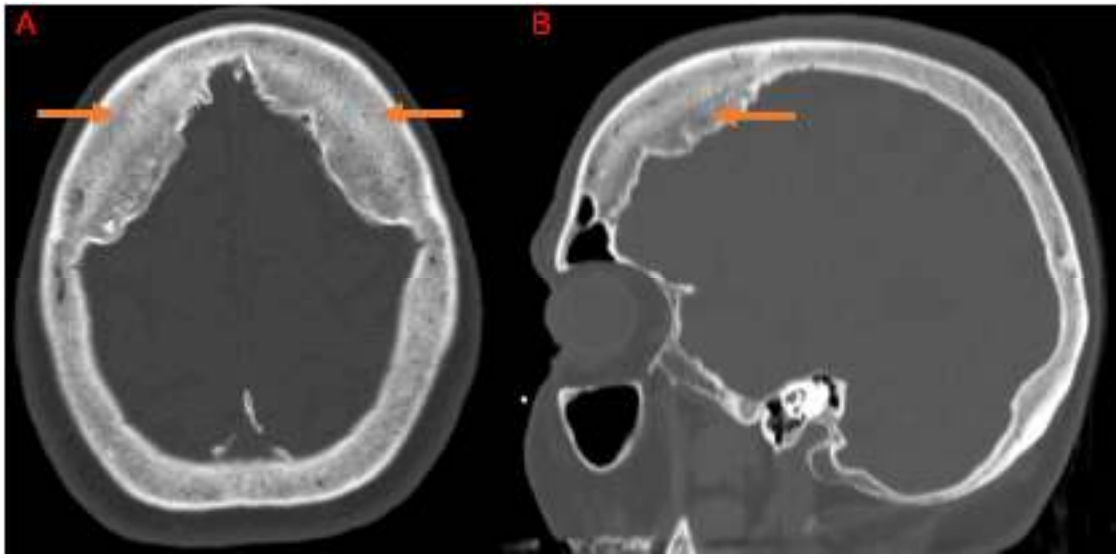

Figure 3. No prior imaging was available for comparison. Therefore, head CT was performed for evaluation. This showed diffuse thickening of the calvarium, most prominent in the frontal regions, without destructive marrow replacing lesion (A, B).

References

1. Rosemary S, Szakacs J. Hyperostosis Frontalis Interna: Case Report and Review of Literature. *Annals of Clinical & Laboratory Science*. 2004;34:206-20.
2. Chaljub G, Johnson III, R, Johnson Jr., R. et al. Unusually exuberant hyperostosis frontalis interna: MRI. *Neuroradiology*. 1999;41:44–45.
3. Schneeberg N, Woolhandler G, Levine R. The clinical significance of hyperostosis frontalis interna. The *Journal of Clinical Endocrinology & Metabolism*. 1947;7:624–635.
4. Raikos A, Paraskevas G, Yusuf F, et al. Etiopathogenesis of hyperostosis frontalis interna: A mystery still. *Annals of Anatomy*. 2011;193:453-458.
5. Lai S, Tomer N. Hyperostosis fronto-parietalis – radiology mimic of metastasis: A case report. *Radiology Case Reports*. 2021;16:2244-2247.
6. Kang S, Kim J, Kwon S, et al. Brain Metastases Mimicking Hyperostosis Frontalis Interna on 99mTc HDP Bone Scintigraphy. *Clinical Nuclear Medicine*. 2016;41:789-791.

18F-Fluciclovine Activity in Spinal Osteophytes

David Manuel, MD and Rachel Powsner, MD

Boston University School of Medicine

Boston VA Healthcare System.

ABSTRACT

Introduction:

Fluorine-18 (^{18}F) fluciclovine (anti-1-amino-3–18F-fluorocyclobutane-1-carboxylic acid [FACBC]) is a radiolabeled amino acid analog that takes advantage of the amino acid transport upregulation in several types of cancer cells. FACBC is a radiolabeled analog of one form of leucine, L-leucine, which is an essential amino acid.

FACBC is a sensitive marker for recurrent and/or metastatic prostate cancer and was the first PET approved agent for staging recurrent prostate adenocarcinoma.

Physiologic FACBC uptake is seen in the bone marrow (12% of the dose) (1) and has been described as demonstrating mild uptake at sites of degenerative disease as well as intense activity in a benign process in joints. (2)

Methods:

This study retrospectively reviewed all ^{18}F-fluciclovine studies for a 15-month period, for a total of 48 cases, and evaluated uptake within osteophytes within the thoracic and lumbar spine. The severity of osteophyte formation in the spine was graded from no formation up to

extensive formation (more than 6 bridging osteophytes). The intensity of the uptake in the osteophytes was divided into four subsets ranging from no uptake to uptake greater than the uptake in the marrow of adjacent vertebral bodies.

Results:

More than 50% of thoracic and lumbar vertebral osteophytes did not demonstrate any ^{18}F-fluciclovine uptake. Those cases that did demonstrate uptake had only mild uptake (less than or equal to marrow uptake in the associated vertebral bodies).

Conclusion:

These results substantiate prior findings that, at least at sites of osteophyte formation from degenerative change in the spine, that there is little ^{18}F-fluciclovine uptake. This would imply that foci of increased uptake greater than vertebral marrow uptake at sites of degenerative change are more suspicious and may represent concomitant metastatic disease. Further research is warranted to determine if these results can be generalized to other sites of degenerative disease in the skeleton.

References:

1. Axumin prescribing information

2. Gusman, Mariya, et al. "Review of 18F-fluciclovine PET for detection of recurrent prostate cancer." Radiographics 39.3 (2019): 822-841.

Title

Role of Nuclear Medicine in the Evaluation of Renal Graft Dysfunction and Related Complications

Authors

Adithya Hari, MD; Edgar Zamora, MD; Deepak Kalbi, MD; Saeed Ghandili, MD; Eitan Novogrodsky, MD; Esther Rong, MD; Kwang J. Chun, MD

Division of Nuclear Medicine
Department of Diagnostic Radiology
Montefiore Medical Center and the Albert Einstein College of Medicine
1695A Eastchester Rd, Bronx, NY, 10461

Correspondence

Adithya Hari, MD
ahari@montefiore.org
Tel (718) 405-8462 / Fax (718) 824-0625
Montefiore Medical Center
1695A Eastchester Rd, Bronx, NY, 10461

Abbreviations

Renal Transplantation; Kidneys; Renal failure; DDRT; Scintigraphy; Nuclear Medicine; Radiology; Post transplant lymphoproliferative disorders.

Conflict of Interest

None of the authors have any conflicts of interest to disclose nor have received any type of financing related to this manuscript.

Background

Diagnostic imaging has an essential role in the multidisciplinary management of kidney transplantation. Doppler ultrasonography is generally considered the first line modality for evaluation of post-operative graft dysfunction, however, other modalities are often needed for more specific diagnostic evaluation and exclusion of nonrejection causes of allograft dysfunction.

Using radiopharmaceuticals such as ^{99m}Tc mercaptoacetyltriglycine (MAG3) or ^{99m}Tc diethylenetriaminepentaacetic acid (DTPA), renal scintigraphy allows qualitative and quantitative assessment of cortical perfusion, tissue extraction, and excretion [1,2]. Additionally, utilization of angiotensin converting enzyme (ACE) inhibitors or loop diuretics can aid in excluding specific diagnoses such as renal artery stenosis or obstruction, respectively.

Complications of kidney transplantation can be categorized into: 1. Medical—subcategorized as a) Acute tubular necrosis (within minutes to hours), b) Acute rejection (within days), c) Chronic rejection (months to years), d) Drug toxicity (months), and 2. Surgical—subcategorized as a) urinary leak, b) obstruction, c) Infection d) hematoma or e) lymph leak [3]. Additionally, post-transplant patients have a higher risk of developing lymphoproliferative disorders (PTLD), where ^{18}F-FDG-PET/CT helps with diagnosis, management, and posttreatment response evaluation [4,5].

Methods/Approach

This image-rich case-based educational exhibit will review the role and applications of nuclear imaging in evaluation of allogenic graft dysfunction and related complications.

Results

Illustrative examples are provided for a number of clinical scenarios describing various applications of renal scintigraphy. These include examples of acute rejection, acute

tubular necrosis, chronic rejection, drug toxicity, urinary leak, outflow obstruction and PTLD.

Conclusion

Renal scintigraphy is a well proven modality for evaluation of graft dysfunction. Repeat scans could be obtained to therapeutic response evaluation. ^{18}F-FDG PET/CT is instrumental in early diagnosis, management, and follow-up of PTLD.

References:

1. Mujoomdar M, et al. Optimizing Health System Use of Medical Isotopes and Other Imaging Modalities [Internet]. Ottawa (ON): Canadian Agency for Drugs and Technologies in Health; 2012. APPENDIX 2.13, Evaluation of Renal Function Post-Transplant.
2. El Maghraby TA, et al. Quantitative scintigraphic parameters for the assessment of renal transplant patients. European journal of radiology. 1998;28(3):256-69.
3. Sugi MD, et al. Imaging of renal transplant complications throughout the life of the allograft: comprehensive multimodality review. Radiographics. 2019 Sep;39(5):1327-55.
4. Bustami RT, et al. Immunosuppression and the risk of post-transplant malignancy among cadaveric first kidney transplant recipients. American Journal of Transplantation. 2004;4(1):87-93.
5. Dierickx D, et al. The accuracy of positron emission tomography in the detection of posttransplant lymphoproliferative disorder. Haematologica. 2013;98(5):771.

Lymphoscintigraphy Guided Sentinel Lymph Node Biopsy for Oral Squamous Cell Carcinoma

Richard Yu, MD[1], Don Goldstein, MD[1], Matin Imanguli, MD, DDS[2], Jeffrey Kempf, MD, FACR[1,3.]

[1]Department of Radiology, Rutgers, Robert Wood Johnson Medical School, Robert Wood Johnson University Hospital, NJ; [2]Department of Otolaryngology-Head and Neck Surgery, Robert Wood Johnson Medical School; [3]Nuclear Radiology Section, Department of Radiology, Rutgers, Robert Wood Johnson Medical School, Robert Wood Johnson University Hospital, New Brunswick, New Jersey.

Background: Oral squamous cell carcinoma (OSCC) is a malignancy of the squamous epithelium of the oral cavity, and is the sixth most common malignancy worldwide, with a high reported mortality rate. Cervical lymph node involvement is an important prognostic factor in patients with OSCC, with the incidence of occult nodal metastases at presentation reported to be approximately 30% in patients with clinically node negative OSCC. Currently, the standard of care for lesions with regional spread is resection of the index tumor with elective neck dissection (END). Unfortunately, END is invasive and associated with significant morbidity. The concept of sentinel lymph node mapping is currently used for some breast cancer and melanoma patients, and currently used in T1-2 N0 OSCC in many countries with slower adoption in the United States. In this exhibit we will review our early experience and protocol for Sentinel Lymph Node Mapping, including injection technique, pre-operative imaging including SPECT/CT and cutaneous marking, and present some representative cases.

Methods: Tc-99m sulfur colloid is employed, filtered in our department with standard 0.22-um filtration. To reduce the pain of injection and potential patient movement during injection, patients are administered 10% lidocaine gel approximately 30 minutes prior to injection. The radiotracer is administered at two-four sites about the lesion with superficial, submucosal injections in a total volume of 1cc in 1mCi (37MBq). Upon completion of injections, the patient rinses their oral cavity without swallowing to reduce salivary contamination. Immediate dynamic imaging of the head and neck is acquired, followed by immediate, planar anterior/posterior, and right/left lateral static images. SPECT/CT of the head and neck is then performed (details in exhibit). Thus far, a sentinel lymph node has been found for each case. The sentinel LN is marked over the patient's skin and this information is provided to the surgeon, who performs same-day resection of the index tumor and SLNB.

Results: Thus far we have performed OSCC lymphoscintigraphy in 16 patients. Some representative patients with T1-2N0 OSCC will be presented. For example: A 58-year-old male with biopsy-confirmed SCC of the left upper maxillary gingiva. Dynamic imaging showed prompt migration to a left neck sentinel lymph node which was localized to a left level 1B submandibular node on SPECT-CT. A second patient: 45-year-old woman with biopsy-confirmed SCC of the left side of the tongue. Dynamic imaging showed migration to a level 2 node in the left maxillary/mandible region, with additional propagation to a left level 3 node. Same-day operative resection and pathological evaluation showed sentinel lymph nodes negative for malignancy in both patients, sparing the need for END.

Conclusion: Lymphoscintigraphy and sentinel lymph node localization can be helpful for patients with early stage N0 oral cavity squamous cell carcinoma. In this exhibit we present our protocol and some representative cases from our early experience of sentinel lymph node mapping and localization for early T1-2 N0 oral cavity squamous cell carcinoma.

Title

Aggressive Metastatic Recurrence of Hepatocellular Carcinoma Following Upper Extremity Trauma: Bone Scintigraphy and CT Correlation

Authors

Edgar Zamora, MD; Louisiana Rivera Valladares, MD; Ukuemi Edema, MD; Aspan Shokrekhuda, MD; Moisés A Zamora, MD; Leonard M Freeman, MD

Background: Hepatocellular carcinoma (HCC) is the most common type of primary liver malignancy, and a leading cause of cancer related deaths in the United States (1). HCC is associated with cirrhosis, hepatitis C virus infection, and alcohol abuse (2), with the majority of patients presenting with advanced disease at the time of diagnosis. Accurate staging is, therefore, essential for initial management strategy planning (3). Extrahepatic metastases most commonly manifest in lung tissue, portal vasculature, and locoregional lymph nodes (4). While relatively less common, bone metastases may present in patients with advanced disease, although usually in concomitance with non-osseous metastases (2). Diagnostic evaluation typically includes contrast-enhanced computed tomography (CT) or magnetic resonance imaging (MRI) of the abdomen. Bone scintigraphy is typically individualized in patients with equivocal osseous lesions or those at higher risk for metastatic osseous disease (5,6). **Methods:** This exhibit will illustrate an unusual case of metastatic recurrence in a patient with hepatocellular carcinoma, following trauma of a distal upper extremity, where correlation with bone scintigraphy and other radiologic studies was essential for diagnosis. **Results:** A man in his early 60's presented to our institution with a two-month history of persistent left hand swelling with

worsening pain after falling twice on an outstretched left hand. The patient had been on clinical remission of HCC for approximately one year, following partial segmentectomy and transarterial chemoembolization of a 2.3 cm hepatic lesion. Anteroposterior plain radiograph of the left wrist showed soft tissue edema and comminuted displaced fracture of the distal end of the left radius with erosion of the carpus and third metacarpal base. CT showed synovial thickening and osseous erosion in the left wrist. Ultrasound imaging revealed a soft tissue mass in the left wrist involving the third metacarpal bone with hypoechogenic polylobulated features associated with comminuted fracture. Differential diagnosis included inflammatory arthritis, osteoarthritis, osteolysis syndrome, or metastatic disease. Whole-body bone scintigraphy was performed for further evaluation, showing diffuse increased activity involving osseous tissues in the left wrist, in a distribution reminiscent of reflex sympathetic dystrophy. The patient underwent ultrasound-guided biopsy and surgical debridement of the left wrist revealing metastatic moderate to poorly differentiated hepatocellular carcinoma infiltrating lamellar tissue of the third metacarpal bone.

Summary: Scintigraphic bone findings in this case were equivocal for malignancy and, despite correlation with CT, the clinical scenario was indeterminate for malignancy. Histopathological evaluation of the left wrist revealed localized aggressive osseous recurrence as an exceedingly rare presentation of HCC after traumatic injury. It is yet unclear whether trauma contributed to proliferation of “dormant” micrometastases and development of fully blown metastatic recurrence. However, distal osseous recurrence following trauma has been described in association with other malignancies, such as

lung cancer (7,8) with some authors suggesting that an increased vascularity and inflammation resulting from trauma may create a more ideal environment for metastatic proliferation (8).

References

1. Centers for Disease Control and Prevention (CDC). Hepatocellular carcinoma - United States, 2001-2006. MMWR Morb Mortal Wkly Rep. 2010 May 7;59(17):517–20.
2. Katyal S, Oliver JH, Peterson MS, Ferris JV, Carr BS, Baron RL. Extrahepatic metastases of hepatocellular carcinoma. Radiology. 2000 Sep;216(3):698–703.
3. Lin S, Hoffmann K, Schemmer P. Treatment of hepatocellular carcinoma: a systematic review. Liver Cancer. 2012 Nov;1(3–4):144–58.
4. Abbas A, Medvedev S, Shores N, Bazzano L, Dehal A, Hutchings J, et al. Epidemiology of metastatic hepatocellular carcinoma, a nationwide perspective. Dig Dis Sci. 2014 Nov;59(11):2813–20.
5. Jin Y-J, Lee HC, Lee D, Shim JH, Kim KM, Lim Y-S, et al. Role of the routine use of chest computed tomography and bone scan in staging workup of hepatocellular carcinoma. J Hepatol. 2012 Jun;56(6):1324–9.
6. Koneru B, Teperman LW, Manzarbeitia C, Facciuto M, Cho K, Reich D, et al. A multicenter evaluation of utility of chest computed tomography and bone scans in liver transplant candidates with stages I and II hepatoma. Ann Surg. 2005 Apr;241(4):622–8.
7. Walter ND, Rice PL, Redente EF, Kauvar EF, Lemond L, Aly T, et al. Wound healing after trauma may predispose to lung cancer metastasis: review of potential mechanisms. Am J Respir Cell Mol Biol. 2011 May;44(5):591–6.
8. El Saghir NS, Elhajj II, Geara FB, Hourani MH. Trauma-associated growth of suspected dormant micrometastasis. BMC Cancer. 2005 Aug 4;5:94.

Title

Heterotopic ossification in critically ill COVID-19 patients: radiologic and scintigraphic manifestations

Authors

Edgar Zamora, MD[1]; Kwang J. Chun, MD[1]; Adithya Hari, MD[1]; Sean Boone, MD[1]; Zina Ricci, MD[2]; Beverly Thornhill, MD[3]; Jenna Le, MD[3]

[1] Division of Nuclear Medicine
Department of Diagnostic Radiology
Montefiore Medical Center and the Albert Einstein College of Medicine
1695A Eastchester Rd, Bronx, NY, USA

[2] Division of Abdominal Imaging
Department of Radiology
Montefiore Medical Center and the Albert Einstein College of Medicine
111 E. 210th Street, Bronx, NY, USA

[3] Division of Musculoskeletal Imaging
Department of Diagnostic Radiology
Montefiore Medical Center and the Albert Einstein College of Medicine
111 E 210th Street, Bronx, NY, USA

Correspondence

Edgar Zamora, MD
ezamora@montefiore.org
Tel (718) 405-8462 / Fax (718) 824-0625
Montefiore Medical Center
1695A Eastchester Rd, The Bronx, NY, 10461

Keywords

Heterotopic Ossification; COVID-19; joint pain and stiffness; immobility; Nuclear Medicine; Radiology

Conflict of Interest

None of the authors have any conflicts of interest to disclose nor have received any type of financing related to this manuscript.

Background: Heterotopic ossification (HO) is a pathologic process leading to inappropriate bony growth in extra-skeletal tissue. It typically manifests in adults following trauma, surgery, or neurological insult and is associated with various predisposing factors and activation of inflammatory pathways (1). Coronavirus disease 2019 (COVID-19) is an infectious disease that may lead to severe inflammatory response syndrome (SIRS) among other complications (2). HO has been reported in critically ill COVID-19 patients, with a fourfold higher incidence among COVID-19 patients compared to non-COVID patients with acute respiratory distress syndrome (1,3,4). Radiologic correlation is often indicated as HO can mimic a neoplastic process on physical examination. HO is commonly evaluated and detected on radiographs or CT scan. Additionally, three-phase bone scintigraphy is a known tool for the pre-surgical evaluation of status of bone maturation (5). Imaging diagnosis of HO at an earlier stage is critical for expeditious physical rehabilitation and appropriate radiological follow-up leading to improved long-term functionality. The authors present two cases from an academic medical institution in a hot zone of the Bronx, New York, where three-phase bone scintigraphy with SPECT/CT and other radiologic studies have been useful in early recognition and follow-up of HO in COVID-19 patients recently discharged from the ICU. **Methods/Approach:** This exhibit illustrates cases of HO in critically ill COVID-19 patients. **Results:** Two patients with severe COVID-19 pneumonia complicated by HO were identified. A 66 year-old-man was hospitalized in the ICU for 1 month for treatment of respiratory failure secondary to COVID-19 and subsequently complained of pain and stiffness involving the right knee and left elbow, for which he was referred for three-phase bone scintigraphy. Planar bone scintigraphy with SPECT/CT revealed new and active dystrophic calcification involving periarticular musculotendinous tissues corresponding to the reported sites of pain. The patient's medical management was optimized with rigorous physical therapy and surgical resection delay based on the active bone formation status. The second patient, a 57 year-old-woman, was admitted to the ICU for treatment of COVID-19 pneumonia with respiratory failure. Following discharge, a contrast-enhanced CT showed a poorly defined enhancing periarticular focus which ossified on follow-up exam. **Conclusions:** Heterotopic ossification is clinically identified as pain, swelling, and/or progressive stiffening of the affected site. Its pathophysiology is diverse based on site of involvement, and it has been associated with activation of inflammatory pathways. COVID-19 may stimulate a similar cascade of events and accelerate the process of heterotopic bone formation in predisposed patients. HO can lead to severe morbidity if left untreated, hence the importance of its early diagnosis and management. Radiographic correlation is important for prompt diagnosis and exclusion of malignant processes that may manifest similar clinical findings. Plain radiograph is often the initial imaging study, although CT is more specific and can be used for interval follow-up. Early

lesions may appear as low-attenuation densities on CT which readily enhance after contrast administration, and typically show increased blood flow on early dynamic bone scintigraphy. Three-phase bone scintigraphy can be used to monitor state of bone formation for pre-surgical planning.

References

1. Meyers C, Lisiecki J, Miller S, Levin A, Fayad L, Ding C, et al. Heterotopic Ossification: A Comprehensive Review. JBMR Plus. 2019 Apr;3(4):e10172.

2. Kabeerdoss J, Pilania RK, Karkhele R, Kumar TS, Danda D, Singh S. Severe COVID-19, multisystem inflammatory syndrome in children, and Kawasaki disease: immunological mechanisms, clinical manifestations and management. Rheumatol Int. 2021 Jan;41(1):19–32.

3. Stoira E, Elzi L, Puligheddu C, Garibaldi R, Voinea C, Chiesa AF. High prevalence of heterotopic ossification in critically ill patients with severe COVID-19. Clin Microbiol Infect [Internet]. 2021 Jan 15 [cited 2021 Mar 10]; Available from: https://www.ncbi.nlm.nih.gov/pmc/articles/PMC7833636/

4. Herridge MS, Cheung AM, Tansey CM, Matte-Martyn A, Diaz-Granados N, Al-Saidi F, et al. One-year outcomes in survivors of the acute respiratory distress syndrome. N Engl J Med. 2003 Feb 20;348(8):683–93.

5. Drane WE. Myositis ossificans and the three-phase bone scan. AJR Am J Roentgenol. 1984 Jan;142(1):179–80.

Title

^{18}F-FDG PET/CT: Initial Staging and Treatment Response Evaluation of Primary Pulmonary Synovial Sarcoma

Deepak Kalbi, MD; Edgar Zamora, MD; Louisiana Rivera Valladares; Ana Y Valdivia, MD; Kwang J Chun, MD

Background: Primary lung malignancies comprise a heterogeneous group of neoplasms most commonly arising from epithelial tissue and often associated with high mortality rates (1). Mesenchymal lung neoplasms, in contrast, are exceedingly rare and often associated with more aggressive behavior. Among various subtypes of mesenchymal lung neoplasms, primary pulmonary synovial sarcoma (PSS) is a rare entity (2,3) usually manifesting in young adults, and comprising approximately 0.013–1.1% of all lung malignancies (4–6). FDG-PET/CT is a well-proven diagnostic imaging modality for evaluation of pulmonary cancer, however, its use for pulmonary synovial sarcoma has been rarely described and its value for staging and treatment response evaluation is yet to be elucidated. The authors seek to contribute to the body of knowledge by describing the use FDG-PET/CT for initial staging and post-chemotherapy response evaluation of PSS at our institution. **Methodology:** This exhibit is an image-rich presentation illustrating the use of FDG-PET/CT in initial staging and treatment response evaluation of PSS. **Results:** A female patient in her early thirties presented for evaluation of shortness of breath and chest pain. CT of the chest revealed a large heterogeneously enhancing pulmonary mass with punctate calcifications within the left lower hemithorax. Subsequent core-needle biopsy revealed PSS with positive immunohistochemistry for BCL-2, EMA, CD56, and D2-40. Initial FDG-PET/CT with 9.3 mCi of ^{18}F-FDG revealed mild activity within the mass measuring 8.4 x 4.3 cm, SUV_{max} 3.0 (hepatic SUV_{mean} 2.5), and a left pleural effusion with left lower lobe collapse. The patient subsequently presented after completing three cycles of chemotherapy. Follow-up FDG-PET/CT was performed with 8.8 mCi of ^{18}F-FDG, revealing decrease in size and activity of the mass measuring 7.7 x 3.0 cm, with SUV_{max} 2.0 (hepatic SUV_{mean} 2.5). When normalized with the liver SUV_{mean} measurements, the lesion was approximately 33% less FDG-avid following treatment. The patient showed further improvement on subsequent conventional diagnostic imaging studies. **Conclusions:** Primary lung synovial sarcomas are rare neoplasms arising from mesenchymal lung tissue. Similar to the patient presented, PSS usually manifest in young adults without preference for sex or laterality–presenting within either hemithorax (7). Prior case report studies have shown similar degrees of mild/moderate heterogeneous activity that is more prominent than corresponding liver SUV_{mean} (8–10), usually forming well-demarcated nonencapsulated lesions that may spread within the bronchi but rarely infiltrate bronchial epithelium (4,7). Our findings indicate that FDG-PET may be a useful modality for both initial staging and treatment response evaluation of these patients.

References

1. Spectrum of Lung Adenocarcinoma - PubMed [Internet]. [cited 2021 Aug 14]. Available from: https://pubmed.ncbi.nlm.nih.gov/31200873/

2. Hartel PH, Fanburg-Smith JC, Frazier AA, Galvin JR, Lichy JH, Shilo K, et al. Primary pulmonary and mediastinal synovial sarcoma: a clinicopathologic study of 60 cases and comparison with five prior series. Mod Pathol. 2007 Jul;20(7):760–9.

3. Bhattacharya D, Datta S, Das A, Halder KC, Chattopadhyay S. Primary pulmonary synovial sarcoma: A case report and review of literature. Int J Appl Basic Med Res. 2016;6(1):63–5.

4. Gołota J, Osowiecka K, Orłowski T. Primary pulmonary sarcoma – long-term treatment outcomes and prognostic factors. Kardiochir Torakochirurgia Pol. 2018 Sep;15(3):162–9.

5. Martini N, Hajdu SI, Beattie EJ. Primary sarcoma of the lung. J Thorac Cardiovasc Surg. 1971 Jan;61(1):33–8.

6. Guccion JG, Rosen SH. Bronchopulmonary leiomyosarcoma and fibrosarcoma. A study of 32 cases and review of the literature. Cancer. 1972 Sep;30(3):836–47.

7. Panigrahi MK, Pradhan G, Sahoo N, Mishra P, Patra S, Mohapatra PR. Primary pulmonary synovial sarcoma: A reappraisal. J Cancer Res Ther. 2018 Jun;14(3):481–9.

8. Shah D, Odedra P. Primary Pleuropulmonary Synovial Sarcoma on Fluorodeoxyglucose Positron Emission Tomography-Computed Tomography Scan. Indian J Nucl Med. 2017;32(4):340–2.

9. Kim GH, Kim MY, Koo HJ, Song JS, Choi C-M. Primary Pulmonary Synovial Sarcoma in a Tertiary Referral Center: Clinical Characteristics, CT, and 18F-FDG PET Findings, With Pathologic Correlations. Medicine (Baltimore). 2015 Aug 28;94(34):e1392.

10. Harisankar CNB, John J, Gangadharan KV. Fluoro deoxyglucose positron emission tomography-computerized tomography in primary staging and response assessment of a rare case of primary pleural synovial sarcoma. Indian J Nucl Med. 2015 Mar;30(1):62–4.